JGR Biogeosciences

RESEARCH ARTICLE
10.1029/2020JG006159

Potential of Sun-Induced Chlorophyll Fluorescence for Indicating Mangrove Canopy Photosynthesis

Xudong Zhu[1,2], Yuwen Hou[1], Yongguang Zhang[3], Xiaoliang Lu[4], Zhunqiao Liu[4], and Qihao Weng[5]

[1]Taiwan Strait Marine Ecosystem National Observation and Research Station, Key Laboratory of the Coastal and Wetland Ecosystems (Ministry of Education), College of the Environment and Ecology, Coastal and Ocean Management Institute, Xiamen University, Xiamen, Fujian, China, [2]Southern Marine Science and Engineering Guangdong Laboratory (Zhuhai), Zhuhai, Guangdong, China, [3]International Institute for Earth System Science, Nanjing University, Nanjing, Jiangsu, China, [4]State Key Laboratory of Soil Erosion and Dryland Farming on the Loess Plateau, Institute of Soil and Water Conservation, Northwest A&F University, Yangling, Shaanxi, China, [5]Department of Earth and Environmental Systems, Center for Urban and Environmental Change, Indiana State University, Terre Haute, IN, USA

Key Points:

- First continuous coordinated measurements of sun-induced chlorophyll fluorescence (SIF) and eddy covariance in mangrove is presented
- SIF serve as a potential remotely sensed indicator of tracking diurnal/seasonal variation in mangrove gross primary productivity (GPP)
- Environmental stresses tend to weaken mangrove SIF-GPP correlation

Supporting Information:

- Supporting Information S1

Correspondence to:
X. Zhu,
xdzhu@xmu.edu.cn

Citation:
Zhu, X., Hou, Y., Zhang, Y., Lu, X., Liu, Z., & Weng, Q. (2021). Potential of sun-induced chlorophyll fluorescence for indicating mangrove canopy photosynthesis. *Journal of Geophysical Research: Biogeosciences*, *126*, e2020JG006159. https://doi.org/10.1029/2020JG006159

Received 6 NOV 2020
Accepted 18 FEB 2021

Author Contributions:

Conceptualization: Xudong Zhu, Qihao Weng
Formal analysis: Xudong Zhu, Yuwen Hou, Xiaoliang Lu, Zhunqiao Liu
Funding acquisition: Xudong Zhu
Investigation: Xudong Zhu, Yuwen Hou
Methodology: Xudong Zhu, Yongguang Zhang, Xiaoliang Lu, Zhunqiao Liu
Project Administration: Xudong Zhu
Resources: Xudong Zhu
Software: Yongguang Zhang
Visualization: Xudong Zhu, Yuwen Hou
Writing – original draft: Xudong Zhu, Qihao Weng
Writing – review & editing: Xudong Zhu, Yuwen Hou, Yongguang Zhang, Xiaoliang Lu, Zhunqiao Liu, Qihao Weng

Abstract Accurate characterization of gross primary productivity (GPP) is critically important in assessing mangrove carbon budgets, but the current knowledge of the temporal variations of GPP in evergreen mangroves is very limited. Remote sensing of sun-induced chlorophyll fluorescence (SIF) has emerged as a promising approach to approximating GPP across ecosystems, but its capability for tracking GPP in evergreen mangroves has not been assessed. The SIF-GPP link at a subtropical mangrove and its environmental controls are explored using 1-year time-series measurements from tower-based hyperspectral and eddy covariance systems. Both the relationship between SIF and GPP as well as that between SIF_y (SIF yield: the ratio of SIF over absorbed photosynthetically active radiation [APAR]) and LUE (light use efficiency: the ratio of GPP over APAR) at diurnal and seasonal time scales are analyzed. The temporal variations of SIF and GPP shared overall similar changing patterns, but their functional relationship tended to be time scale-dependent. Midday depressions in SIF were observed when environmental stresses occurred around noon (including excess light and high VPD), and the strength of the SIF-GPP link was affected by changing environmental conditions. The SIF_y-LUE relationship was temporally more dynamic, tending to match during midday hours but diverge from each other during morning and afternoon hours. These findings confirm SIF can serve as a potential remotely sensed indicator of mangrove canopy photosynthesis. This paper provides the first, high temporal-resolution, continuous SIF measurements in mangroves, and highlights the importance of the impacts of environmental conditions on the SIF-GPP relationship.

1. Introduction

As typical tropical and subtropical coastal wetland ecosystems, mangroves are characteristic of rich carbon storage and strong carbon sequestration potential (Atwood et al., 2017) and thus have been recognized as important and effective long-term blue carbon sinks in climate change mitigation (Howard et al., 2017; Nellemann & Corcoran, 2009). Mangroves may experience a variety of environmental stresses, including periodical inundation (Crase et al., 2015), high salinity (Song et al., 2011), wastewater pollution (Jiang et al., 2018), all of which are temporally varying and/or spatially heterogeneous. Moreover, due to the inaccessibility to mangroves and notoriously difficult field environments, manual monitoring of mangroves on a regular basis is impractical. Therefore, it is challenging to accurately assess mangrove carbon fluxes that vary temporally and spatially (Alongi, 2012, 2014). Gross primary production (GPP) is the beginning of vegetation carbon biogeochemical cycle and the key indicator of vegetation carbon fluxes, and thus accurate characterization of photosynthesis is critically important in assessing carbon dynamics and carbon sequestration potential.

Unfortunately, GPP cannot be directly observed but must be simulated by process-based ecosystem productivity models (e.g., BEPS; Liu et al., 1997) or empirically estimated from other measurements. One empirical approach is to estimate GPP from continuous measurements of net ecosystem exchange of CO_2 (NEE) using

the eddy covariance (EC) methodology (Baldocchi et al., 2001), in which GPP can be derived through partitioning measured NEE. EC has been used for various ecosystems including mangroves (Barr et al., 2010; Liu & Lai, 2019; Zhu et al., 2019), since it provides a long term, continuous, and near-direct assessment of ecosystem-atmospheric NEE. Another empirical approach to estimate GPP is based on spectral measurements from remote sensors by linking optical signals with ecosystem photosynthesis, mostly through light use efficiency (LUE) models (Gamon, 2015). The LUE-based GPP models might work better for deciduous or annual vegetation, since their photosynthesis is mainly regulated by canopy greenness that can be well tracked with commonly used vegetation indices (VIs) like normalized difference vegetation index (NDVI; Myneni & Williams, 1994) and enhanced vegetation index (EVI; Huete et al., 2002). For evergreen vegetation like mangroves with relatively stable canopy greenness, the seasonality of GPP is largely decoupled with these reflectance-based VIs (Barr et al., 2013; Zhu et al., 2019). As a complement to reflectance-based VIs, sun-induced fluorescence (SIF) has recently emerged as a promising spectral approach to approximating GPP given that the strong SIF-GPP correlation has been confirmed across spatial scales with spaceborne (Frankenberg et al., 2011; Guanter et al., 2014; Sun et al., 2018), airborne (Damm et al., 2014; Zarco-Tejada et al., 2013), and ground-based (Miao et al., 2018; Yang et al., 2015) platforms.

SIF is a chlorophyll fluorescence emitted by photosynthetic pigments after solar light absorption. SIF carries direct information on the actual electron transport in the light reactions of photosynthesis and is mechanically linked with GPP (Gu et al., 2019; Porcar-Castell et al., 2014). In practice, SIF can be retrieved within deep and narrow atmospheric absorption bands where a small fluorescence signal is technically discernible from large background solar radiation (Meroni et al., 2009). Although many previous studies have empirically shown a close relationship between SIF and GPP across ecosystems and platforms, the knowledge of the controlling mechanisms of SIF signal and its linkage with GPP is still limited. First, although SIF and GPP are closely coupled at the physiological level, there is theoretically no universal scaling relationship between each other because several space- and time-dependent physiological and canopy-structure factors affect how measured SIF is related to GPP (Gu et al., 2019; He et al., 2017; Zhang et al., 2019). For example, the absorbed photon energy in the light reactions excites Chl molecules, and then the excitation energy is consumed by three main pathways including photochemical processes, fluorescence emissions, and heat dissipation through non-photochemical quenching, all of which are temporally dynamic and under different physiological controls (Porcar-Castell et al., 2014). Although there is a close connection among three pathways, one can only physiologically interpret the link between two processes when one or more of these three processes are determined. Thus, the SIF-GPP relationship is also a function of environmental stresses (Ač et al., 2015; Maxwell & Johnson, 2000). Second, both linear and nonlinear empirical functions have been proposed to represent the SIF-GPP relationships, but it is unclear which one works better in estimating GPP from SIF. Although many previous studies have reported linear SIF-GPP relationships, in particular, with spaceborne sensors (Frankenberg et al., 2011; Guanter et al., 2014; Sun et al., 2017), this linear relationship on a global scale is likely to be an artifact due to temporal and spatial aggregation of original SIF signals (Gu et al., 2019; Magney et al., 2019). In fact, nonlinear asymptotic SIF-GPP relationships have also been reported in both spaceborne (Li et al., 2018) and ground-based (Paul-Limoges et al., 2018) studies. Therefore, large-scale SIF-GPP patterns might not represent actual SIF-GPP correlations at plant and ecosystem scales (Damm et al., 2015). Third, spaceborne and airborne remote sensing generally provide snapshots of SIF under clear sky conditions, and thus there is an under-sampling of SIF under other light conditions, like diffuse light. Without temporally continuous SIF signals, it is difficult to fully assess the influence of light conditions on SIF and its correlation with GPP, which is non-trivial given the significant contribution of diffuse light to GPP (Mercado et al., 2009; Zhang et al., 2011). Fourth, there is limited knowledge of the relationship between the quantum yield of SIF (SIF_y: the ratio of SIF over absorbed photosynthetically active radiation [APAR]) and LUE (the ratio of GPP over APAR), and how this relationship changes with APAR (Miao et al., 2018). Although the SIF-GPP ratio is by definition equivalent to the SIF_y-LUE ratio at instantaneous scales, the SIF-GPP relationship at long-term scales is jointly determined by the SIF_y-LUE relationship and the temporal variations in APAR. Due to much larger variations in APAR than those in both SIF_y and LUE, APAR has been found to be the dominant factor controlling the linear SIF-GPP relationship (Yang et al., 2015). The LUE-APAR relationship has been widely reported across ecosystems (Gitelson & Gamon, 2015; Turner et al., 2003), but the SIF_y-APAR and SIF_y-LUE relationships are rarely investigated and still unclear (Miao et al., 2018; Verma et al., 2017).

In the face of the challenges discussed above, ground-based continuous and concurrent time-series measurements of SIF and GPP (e.g., via EC flux towers) are highly needed to capture both short-term and long-term temporal variations of SIF, GPP and their relationship under different environmental conditions. Although the SIF-GPP correlation has been confirmed in several tower-based field studies, they were conducted largely for croplands (Goulas et al., 2017; Liu et al., 2017) or temperate/boreal forests (Magney et al., 2019; Yang et al., 2015). Until now, we are not aware of any SIF study for mangroves with long-term continuous high-frequency measurements of SIF. Although the empirical linear SIF-GPP relationship has been established in previous tower-based field studies on temperate/boreal forests (Magney et al., 2019; Yang et al., 2015), it is unclear whether this linearity is applicable to subtropical/tropical evergreen forests like mangroves. As low-latitude coastal wetland vegetation, evergreen mangroves are experiencing stronger atmospheric interference (e.g., cloudiness and aerosols) and smaller temperature difference (both diurnal and seasonal). Thus, the responses of SIF and GPP to varying light and temperature conditions might not be obvious. Furthermore, evergreen mangroves have low stomatal conductance and intercellular CO_2 levels, and thus the photosynthetic rates tend to saturate at relatively lower light intensity (Alongi, 2009; Ball, 1996), which could make mangrove's SIF-GPP relationship different from others. Here, based on continuous and concurrent time-series measurements from tower-based hyperspectral and EC systems, we derived and analyzed 1-year temporally continuous high-frequency signals of SIF and GPP at a subtropical mangrove. The main objectives of this study were (1) to explore the diurnal and seasonal variations of mangrove SIF and GPP and their environmental controls; (2) to investigate the empirical relationship between SIF and GPP at diurnal and seasonal time scales; and (3) to examine the influence of different environmental conditions on mangrove SIF-GPP relationships.

2. Materials and Methods

2.1. Field Site

A mangrove forest within an intertidal estuarine wetland of southeastern China was investigated with a variety of in-situ time-series measurements at a mangrove flux tower (23.9240°N, 117.4147°E; Yunxiao mangrove site of ChinaFLUX and USCCC; Figure 1). With a subtropical monsoon climate, this estuarine wetland has an annual mean air temperature of 21.2°C, rainfall of 1,714.5 mm (mostly during spring and summer), and relative humidity of 79% (Lin, 2001). The mangrove forest around the flux tower has dense canopy structure with species composition mainly of *Kandelia obovate*, *Avicennia marina*, and *Aegiceras corniculatum* (Zhu et al., 2019). With irregular semi-diurnal tide (mean tide range of ~2 m), the understory sediment surface at the flux tower is normally inundated twice a day with varying maximal tidal heights (up to ~1 m) (Zhu et al., 2019). This mangrove forest is administrated by the Zhangjiang Estuary Mangrove National Nature Reserve, China, and all permits for our research activities are acquired from them.

2.2. Environmental and Eddy Covariance Measurements

Air temperature and relative humidity were measured above the canopy using an HMP155A sensor (Vaisala), and vapor pressure deficit (VPD) was derived from air temperature and relative humidity (Murray, 1966). Photosynthetically active radiation (PAR) was measured above the canopy using a PQS1 PAR Quantum sensor (Kipp & Zonen). Rainfall was measured above the canopy using a TE525MM Rain Gage (Campbell Scientific, Inc.). Soil temperature was measured at a depth of 20 cm using a soil thermocouple probe (model 109; Campbell Scientific, Inc.). Incoming (SW_{in}) and outgoing (SW_{out}) shortwave radiation were measured above the canopy using a CNR4 Net Radiometer (Kipp & Zonen). Meteorological measurements were recorded using a CR1000 datalogger (Campbell Scientific, Inc.). Tidal surface water level was calculated based on pressure difference from a pair of pressure sensors: one (HOBO U20L-04 Water Level Logger; Onset) was deployed just above sediment surface at the flux tower to measure varying pressures with tidal cycles, and the other (CS106 barometer; Vaisala) was deployed on the flux tower to monitor air pressure. Raw 10-min time series of meteorological and tidal measurements were consistently converted to 30-min data for further analysis.

Mangrove-atmospheric NEE was measured continuously using the EC technique (Baldocchi et al., 2001). The EC system consisted of a three-axis sonic anemometer (CSAT-3; Campbell Scientific, Inc.) and an open

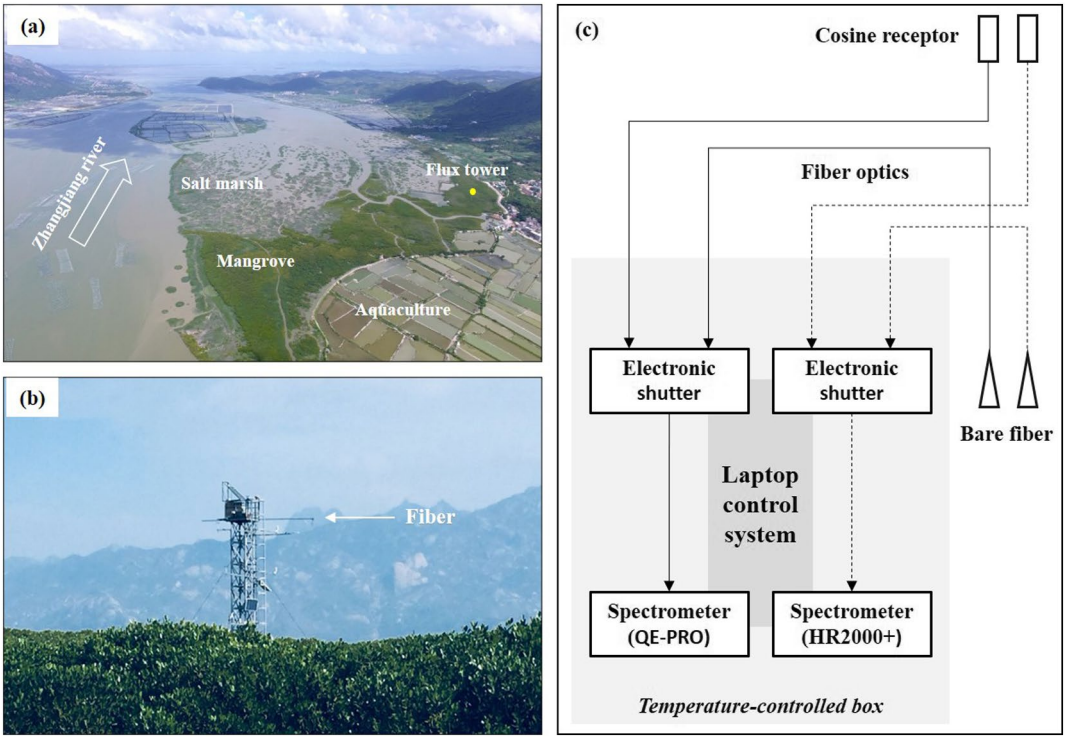

Figure 1. Wetland landscape of the field site (a) and horizontal view of mangrove flux tower (b) deployed for meteorological, eddy covariance, and hyperspectral measurements (for visual reference, the forest strip around the flux tower is ~200-m wide). Various instruments, including two spectrometers, were integrated as shown in the sketch diagram (c) to collect continuous hyperspectral measurements for retrieving SIF and vegetation indices.

path infrared gas analyzer (LI-7500; Li-COR Inc.). Mangrove forests had varying canopy heights averaged at ~4 m (Zhu et al., 2019), and the EC system was mounted on the tower at a height of ~6 m. Raw EC data at 10 Hz was recorded using a CR3000 datalogger (Campbell Scientific, Inc.) and processed to 30-min NEE using the EddyPro6.1 software (Li-COR Inc.). Necessary flux correction (including axis rotation, ultrasonic correction, and frequency response correction) and quality control (including steady-state test, turbulent conditions test, statistical tests, absolute limits test, and rain test) procedures were implemented in EddyPro6.1 to ensure the quality of processed EC data. Nighttime poor flux measurements under insufficient turbulence were filtered out using a friction velocity threshold calculated as in Reichstein et al. (2005). Storage fluxes of CO_2 calculated in EddyPro6.1 using a single-point concentration profile method were also considered in computing NEE. Co-spectral analysis indicated the EC system was able to capture eddy fluxes across the whole range of frequencies. The daytime 30-min ecosystem respiration (Re) was first estimated from daytime soil temperature based on the fitted nighttime Re-soil temperature response curve, and then used for partitioning 30-min GPP from daytime 30-min NEE (more details in Zhu et al. [2019]). Similar to Barr et al. (2013), nighttime NEE values with inundated sediment surface were excluded in fitting the Re-temperature response curve since measured nighttime NEE under inundated conditions was likely lower than actual nighttime Re because respired CO_2 might dissolve into the overlying tidal water and be exported. The LUE (mol mol^{-1}) was calculated as the ratio of GPP and APAR (Equation 1), which is the product of PAR and fraction of APAR (f_{APAR}) (Equation 2). The f_{APAR} was approximately estimated for the canopy based on concurrent measurements of SW_{in} and SW_{out} (Equation 3) (Nichol et al., 2019). The daily GPP and LUE were calculated as the average of 30-min GPP and LUE, respectively. The monthly GPP and LUE were averaged from the daily values.

$$LUE = GPP / APAR \quad (1)$$

$$APAR = PAR \times f_{APAR} \quad (2)$$

$$f_{APAR} = 1 - SW_{out} / SW_{in} \quad (3)$$

2.3. Hyperspectral Measurements and Calculations

Following the FluoSpec2 system (Miao et al., 2018; Yang et al., 2015), two high-accuracy hyperspectral spectrometers were deployed on the mangrove flux tower in December 2017 to acquire long-term continuous hyperspectral measurements for retrieving SIF and VIs (Figure 1). The first hyperspectral spectrometer (QE-PRO, OceanOptics, Inc.), covering the wavelength from 730 to 786 nm with a spectral resolution of 0.1 nm (full width half maximum, FWHM), was used for SIF retrieval at the O_2-A band (760 nm). The second one (HR2000+, OceanOptics, Inc.), covering the wavelength from 200 to 1,100 nm with a spectral resolution of 1.5 nm (FWHM), was used to calculate VIs. Each spectrometer was connected to a pair of upward-facing (irradiance path; collecting signals from the sun) and downward-facing (radiance path; collecting signals from the mangrove canopy) fiber optics (mounted at the height of ~7 m above the canopy), and an inline fiber optic shutter (FOS-2X2-TTL, OceanOptics, Inc.) was embedded between the spectrometer and fiber optic to switch between irradiance and radiance paths. The upward-facing fiber optic attached with a cosine corrector (CC-3-UV-S, OceanOptics, Inc.) had a field of view (FOV) of 180°, while the downward-facing bare fiber optic had a FOV of 25° (footprint of ~3 m in diameter). The spectrometers and inline shutters were housed in a temperature-controlled enclosure.

The spectrometer-shutter system first collected solar irradiance, then collected canopy radiance with shutter switched, and then collected solar irradiance with shutter switched back. To improve signal-to-noise ratio, the system was configured to have an adaptive illumination-dependent integrating time during each collection (<10 s). The system triggered an irradiance-radiance-irradiance measurement cycle every 5 min to acquire one canopy radiance measurement and the mean of two solar irradiance measurements. Radiometric calibrations of the system were performed before data collection: irradiance signals were calibrated using a standard light source (HL-3P-CAL, OceanOptics, Inc.) and radiance signals were calibrated using a standard reflection board (Spectralon®, Labsphere). All measurements were corrected for dark current, and raw data collected by the spectrometers were converted to irradiance (mW m^{-2} nm^{-1}) and radiance (mW m^{-2} nm^{-1} sr^{-1}) (Perez-Priego et al., 2005). For example irradiance, radiance, and apparent reflectance spectra over the course of the day were given in Figure S1. To avoid potential large deviation from the cosine corrector (e.g., self-shading issue from the recessed cavity), we excluded the raw measurements acquired with solar elevation angle <30° (71% data remaining at this stage). Following Cogliati et al. (2015), additional data quality control procedures were applied to filter out poor-quality spectra measurements: (1) collected data were checked not to represent spectrometer saturation values (68% data remaining); (2) poor-quality data were rejected by checking the magnitude and stability of irradiance and radiance within each irradiance-radiance-irradiance measurement cycle, to avoid potential disturbance from cloudy conditions (e.g., a quick cloudy/clear shift) (67% data remaining); (3) too low irradiance (vs. dark current) was rejected to exclude poor-quality measurements under low-illumination conditions (55% data remaining); (4) data acquired with non-optimal integration time (maximum irradiance < half of spectrometer saturation values) were also rejected (33% data remaining). Thus, the availability of valid data reduced from 71% to 33% with higher availability in autumn (57%; how much of the data were valid within this season) and winter (42%) and lower availability in summer (29%) and spring (21%).

SIF at 760 nm was retrieved from the hyperspectral measurement (QE-PRO) in the O_2-A band (atmospheric absorption spectrum) using the spectral fitting method (SFM; Meroni et al., 2009). By assuming both canopy reflectance ($r(\lambda)$) and SIF ($F(\lambda)$) are linear functions of wavelength (λ; nm) in the O_2-A band, SIF can be retrieved from hyperspectral measurements of incident solar irradiance ($E(\lambda)$) and reflected radiance ($L(\lambda)$):

$$L(\lambda) = \frac{r(\lambda)E(\lambda)}{\pi} + F(\lambda) + \varepsilon(\lambda), \lambda \in [757.834, 768.763] \quad (4)$$

where $\varepsilon(\lambda)$ is the model error. In practice, a total of 194 bands within the spectral range between 757.834 and 768.763 nm were used to retrieve SIF at 760.351 nm.

Since photochemical reflectance index (PRI; Gamon et al., 1992) has been often found to scale well with GPP across different ecosystems including evergreens (Garbulsky et al., 2011), the PRI-GPP relationship was also examined here. Specifically, PRI was retrieved from canopy reflectance data at specific wavelengths ($r(\lambda)$) based on incident and reflected spectral signals from HR2000+:

$$\mathrm{PRI} = \left(r_{531} - r_{570}\right) / \left(r_{531} + r_{570}\right) \quad (5)$$

Both SIF and PRI were calculated every 5-min and then averaged to 30-min values for further analyses. Spectral measurements under rainy conditions were excluded. To remove the effect of APAR variation on the SIF-GPP relationship, we also compared LUE with the quantum yield of SIF (SIF_y; J nm^{-1} sr^{-1} mmol^{-1}), which was calculated as the ratio of 30-min SIF and APAR:

$$SIF_y = SIF \,/\, APAR \quad (6)$$

Daily values of SIF, PRI, and SIF_y were calculated by averaging all 30-min values. The monthly values were averaged from the daily values.

3. Results

3.1. Temporal Variations of GPP and LUE

The 30-min GPP showed significant diurnal and seasonal variations from December 2017 to October 2018 (Figure 2a). The magnitude of GPP typically varied from 0 to 25 μmol m^{-2} s^{-1} with the daytime mean GPP of 16.0 μmol m^{-2} s^{-1}. At the diurnal scale, the 30-min GPP showed humped varying patterns with values peaking around noon. At the seasonal scale, the 30-min GPP had the highest and lowest values in spring (daytime mean value of 17.0 μmol m^{-2} s^{-1}) and winter (14.8 μmol m^{-2} s^{-1}), respectively. The daily GPP (average of 30-min values), ranging from 3.52 to 21.8 μmol m^{-2} s^{-1}, also had a strong variation over the year with the highest and the lowest mean daily values in spring (16.9 μmol m^{-2} s^{-1}) and winter (14.7 μmol m^{-2} s^{-1}), respectively (Figure 3a). There were also significant diurnal variations in 30-min LUE values typically varying from 0.01 to 0.04 mol mol^{-1} with the daily average of 0.019 mol mol^{-1}, while there was no obvious seasonal varying pattern in 30-min LUE (Figure 2c). The 30-min LUE tended to show U-shaped diurnal patterns with the values lower around noon and higher at dawn and dusk. The daily LUE varied from 0.010 to 0.054 mol mol^{-1} with an average of 0.020 mol mol^{-1}, and daily LUE was higher in winter (0.023 mol mol^{-1}) than in other seasons (0.019 mol mol^{-1}) (Figure 3b).

3.2. Temporal Variations of SIF and SIF_y

The 30-min SIF varied across time at both diurnal and seasonal scales, and the magnitude typically changed from 0.2 to 1.2 mW m^{-2} nm^{-1} sr^{-1} with the daytime mean of 0.44 mW m^{-2} nm^{-1} sr^{-1} (Figure 2b). Like GPP, the 30-min SIF followed humped diurnal patterns with statistically significant ($p < 0.05$) higher mean values in summer (0.55 mW m^{-2} nm^{-1} sr^{-1}) and autumn (0.54 mW m^{-2} nm^{-1} sr^{-1}) than winter (0.30 mW m^{-2} nm^{-1} sr^{-1}) and spring (0.16 mW m^{-2} nm^{-1} sr^{-1}). The daily SIF, ranging from 0.03 to 1.01 mW m^{-2} nm^{-1} sr^{-1}, varied over the year with statistically significant ($p < 0.05$) higher mean values in summer (0.44 mW m^{-2} nm^{-1} sr^{-1}) and autumn (0.46 mW m^{-2} nm^{-1} sr^{-1}) than in winter (0.32 mW m^{-2} nm^{-1} sr^{-1}) and spring (0.20 mW m^{-2} nm^{-1} sr^{-1}) (Figure 3a). The 30-min SIF_y ranged from 1.0×10^{-4} to 1.3×10^{-3} J nm^{-1} sr^{-1} mmol^{-1} (daily average of 4.1×10^{-4} J nm^{-1} sr^{-1} mmol^{-1}) (Figure 2d), and the daily SIF_y ranged from 4×10^{-6} to 1.2×10^{-3} J nm^{-1} sr^{-1} mmol^{-1} (average of 3.5×10^{-4} J nm^{-1} sr^{-1} mmol^{-1}) (Figure 3b). Same as SIF, the mean values of both 30-min and daily SIF_y were found to be statistically significant ($p < 0.05$) higher in summer and autumn than in winter and spring.

3.3. Correlation Between SIF and GPP

Although there was not good consistency in temporal variations of daily SIF and GPP, the running mean of the daily values indicated that SIF tracked with GPP to a certain extent, where the peaks and troughs of the smoothed curves roughly matched each other (Figure 3a). The strength of the SIF-GPP correlations varied with seasons, with better covariations between 30-min SIF and GPP in summer (correlation

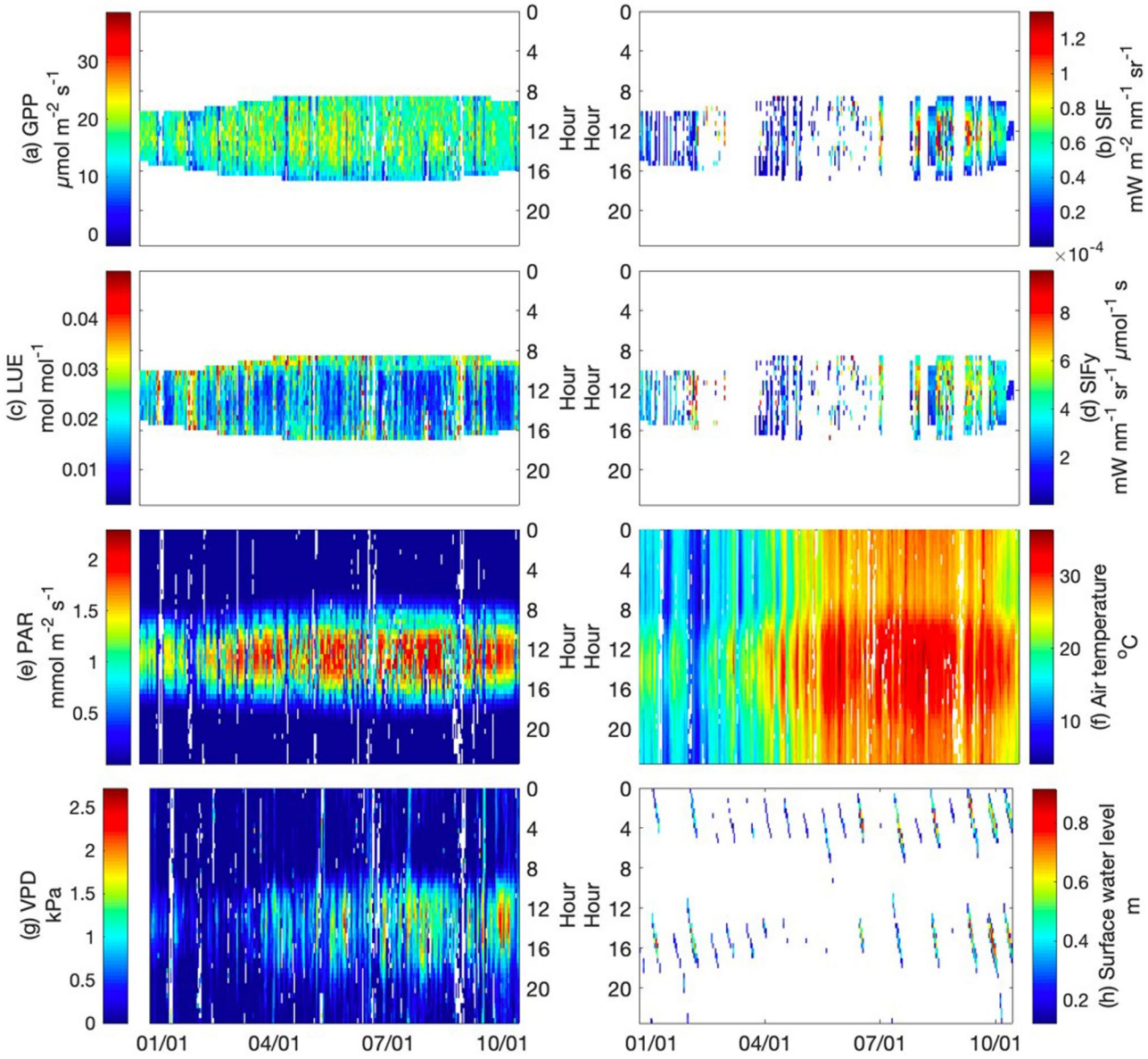

Figure 2. Diurnal and seasonal variations in 30-min measurements of (a) GPP, (b) SIF, (c) LUE, (d) SIF_y, and environmental factors (e–h: PAR, air temperature, VPD, and surface water level) from December 2017 to October 2018. The data with solar elevation angle ≥30° were shown only for the former four variables. Gaps in the data resulted from instrument failure and quality control. GPP, gross primary productivity; LUE, light use efficiency; PAR, photosynthetically active radiation; SIF, sun-induced chlorophyll fluorescence; SIF_y, quantum yield of SIF; VPD, vapor pressure deficit.

coefficient between diurnal mean values, $r = 0.84$, $p < 0.05$) and autumn ($r = 0.82$, $p < 0.05$) (Figure 4). The 30-min GPP followed humped varying patterns across seasons without obvious downregulation around noon, while the diurnal courses of SIF experienced obvious downregulations around noon, in particular for summer and autumn. The positive SIF-GPP relationships at diurnal and seasonal time scales were confirmed by the statistical analysis using 30-min and daily data, respectively (Figures 5a and 5c). Moreover, the positive SIF-GPP relationship was found to be more nonlinear and linear at diurnal and seasonal time scales, respectively. At diurnal time scale, a nonlinear regression ($\mathrm{GPP} = \left(18.7 \times \mathrm{SIF} - 2.93\right) / \left(\mathrm{SIF} + 0.24\right)$) explained 14% of the variations ($p < 0.05$), while at seasonal time scale the SIF-GPP relationship was better described by a linear regression ($\mathrm{GPP} = 14.29 + 4.01 \times \mathrm{SIF}$; $R^2 = 0.17$, $p < 0.05$). The SIF-GPP correlation was comparable with the PRI-GPP correlations at both diurnal (Figure 5a vs. Figure 5b) and seasonal (Figure 5c vs. Figure 5d) time scales. Further analysis of environmental influence on the SIF-GPP correla-

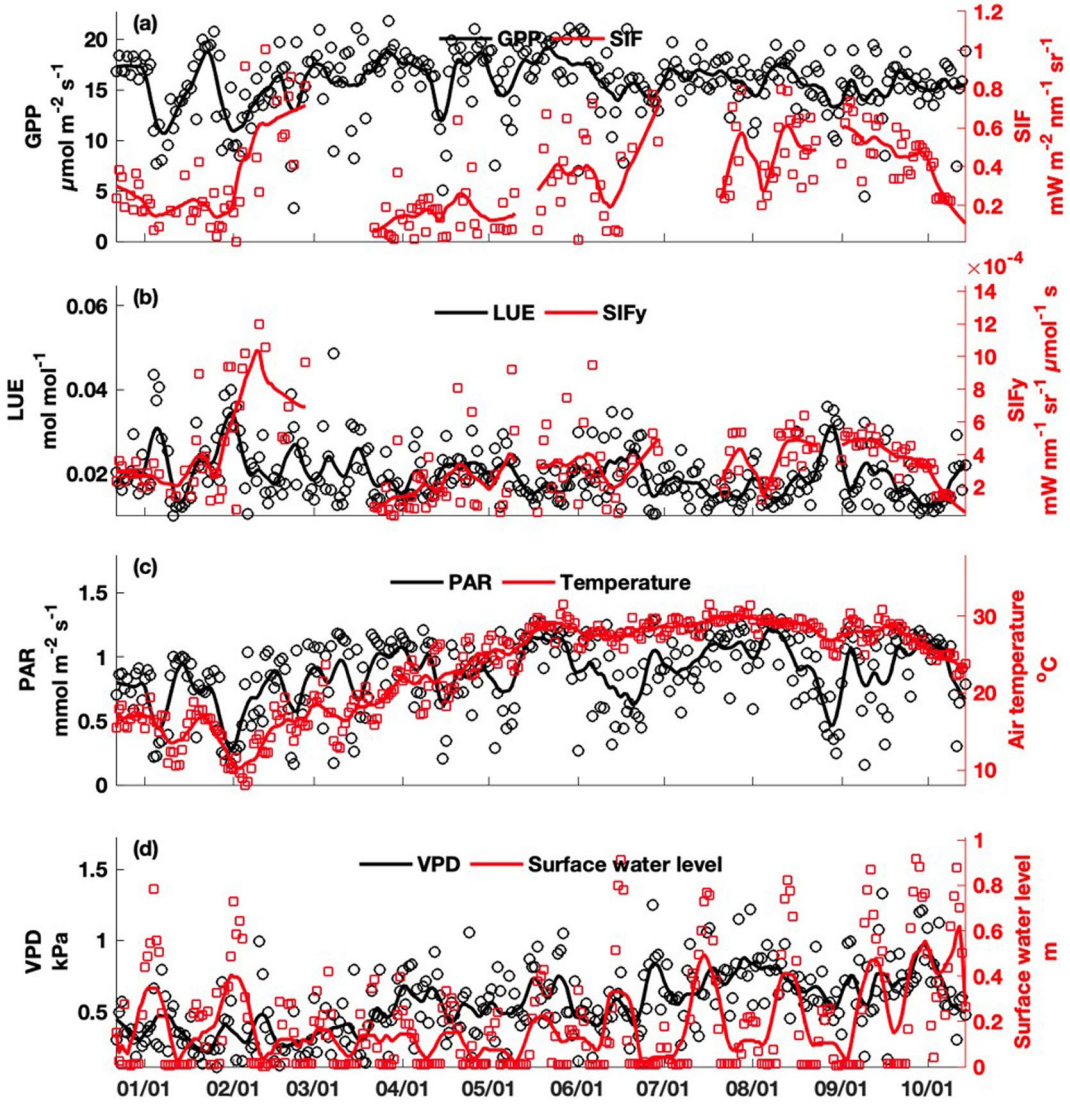

Figure 3. Seasonal variations in daily GPP, SIF, LUE, SIF_y, and environmental factors (PAR, air temperature, VPD, and surface water level) from December 2017 to October 2018. The daily mean values were shown for the variables except for surface water level (using daily maximum values). Lines represented 11 days moving average of daily values. GPP, gross primary productivity; LUE, light use efficiency; PAR, photosynthetically active radiation; SIF, sun-induced chlorophyll fluorescence; SIF_y, quantum yield of SIF; VPD, vapor pressure deficit.

tion indicted that the correlation coefficients between 30-min SIF and GPP were not constant across various environmental gradients (Figure 6). Among the five investigated environmental variables (PAR, air temperature, VPD, surface water salinity, and surface water level), the impacts of VPD on the SIF-GPP relationship were the most obvious with lower SIF-GPP correlations at higher VPD.

3.4. Correlation Between SIF_y and LUE

The correlation between SIF_y and LUE was found to be weaker than the SIF-GPP correlation. At seasonal time scale, both of the time series of daily SIF_y and LUE fluctuated a lot, but there was no obvious covariation between them (Figure 3b). At diurnal time scale, the strength of the SIF_y-LUE correlations varied across seasons, with better covariations in spring ($r = 0.72$, $p < 0.05$) and winter ($r = 0.64$, $p < 0.05$) (Figure 7). During the course of the day, 30-min LUE tended to be higher at morning/afternoon hours and lower around noon, although this U-shaped diurnal pattern was not obvious due to the dismissal of early

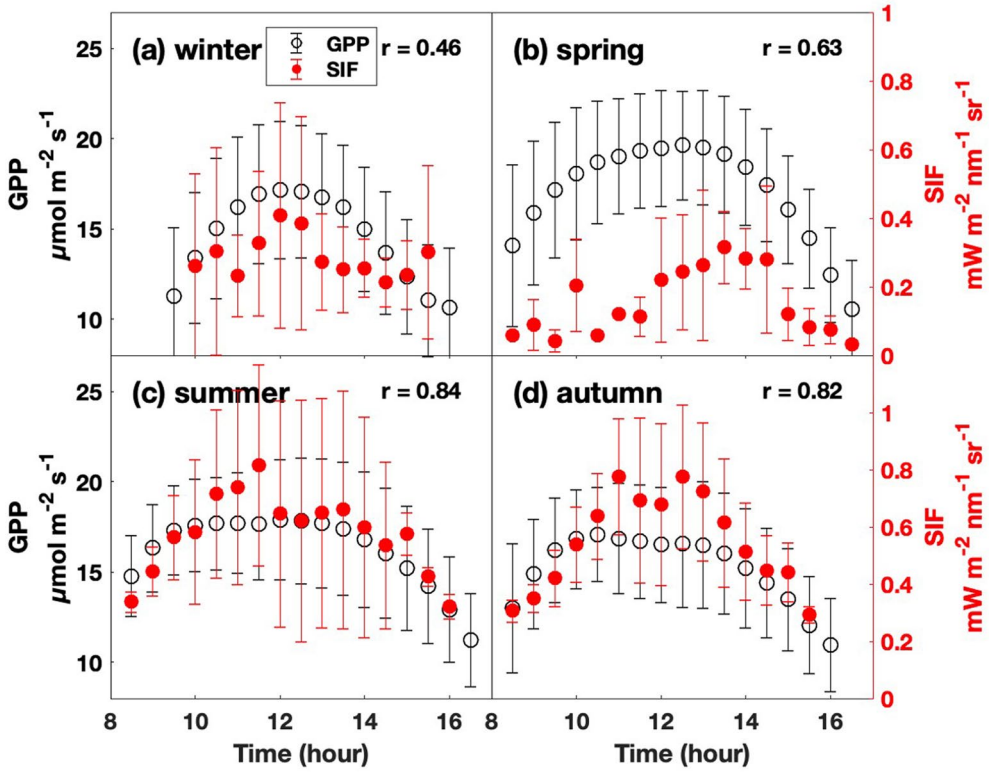

Figure 4. Diurnal mean GPP and SIF across seasons: (a) winter, (b) spring, (c) summer, and (d) autumn. Markers and error bars represented mean values and standard deviations, respectively. Pearson's correlation coefficients (r) between diurnal mean GPP and SIF were calculated for each season (all coefficients were statistically significant at $p < 0.05$). Note the data with solar elevation angle <30° were excluded via quality control. GPP, gross primary productivity; SIF, sun-induced chlorophyll fluorescence.

morning/late afternoon hours with solar elevation angle <30°. For 30-min SIF_y, there was no obvious diurnal variation for each season. The comparison between 30-min SIF_y and LUE indicated that they tended to match during midday hours but diverge from each other during morning and afternoon hours.

4. Discussion

4.1. The SIF-GPP Link and Its Environmental Controls

The relationship between SIF and GPP observed from this study conform to previous understanding that there is a link between photosynthetic CO_2 assimilation and accompanying chlorophyll fluorescence emissions. The coupled SIF-GPP relationship demonstrates the potential of SIF to track the temporal dynamics of GPP in mangroves. Although the SIF-GPP link has been confirmed across ecosystems and platforms, whether the link is linear or nonlinear has not been well understood (Damm et al., 2015; Lee et al., 2015; Yang et al., 2017). Many of previous SIF studies reported a linear SIF-GPP relationship (Magney et al., 2019; Nichol et al., 2019; Yang et al., 2015), but recent studies have also revealed that the SIF-GPP relationship tended to be nonlinear, especially at shorter time scales (Lee et al., 2015; Paul-Limoges et al., 2018; Zhang et al., 2016). Based on 1-year time-series measurements from hyperspectral and EC systems, we were able to better examine the SIF-GPP relationship in mangroves across time scales. The strength of the SIF-GPP linkage at diurnal and seasonal time scales was comparable, but the positive link tended to shift from a nonlinear pattern at diurnal time scale to a linear pattern at seasonal time scale (Figures 5a and 5c). This finding is consistent with previous empirical/modeling studies (Damm et al., 2015; Li et al., 2018; Zhang et al., 2016) showing the functional relationship between SIF and GPP was not consistent across time scales with a trend of being more linear with temporal aggregations. This finding also agrees with recent research

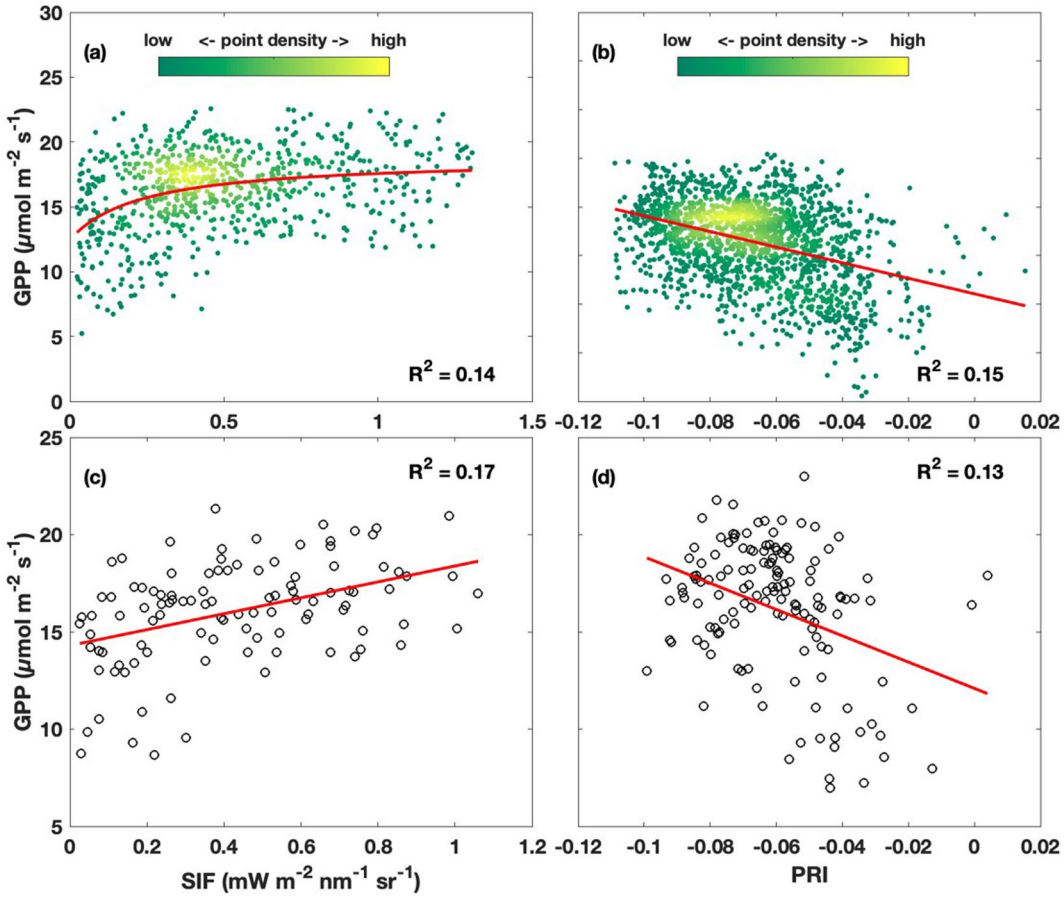

Figure 5. The relationships between GPP and SIF and between GPP and PRI at diurnal (a) and (b) and seasonal (c) and (d) time scales. Statistically significant ($p < 0.05$) fitting curves and corresponding R^2 were also shown. The color bars in the first row indicated point density of 30-min values. GPP, gross primary productivity; PRI, photochemical reflectance index; SIF, sun-induced chlorophyll fluorescence.

review by Gu et al. (2019) demonstrating that nonlinear instantaneous SIF-GPP relationship should in theory move toward more linear when integrated over time.

Midday depression in SIF was observed from our measurements, and this phenomenon was found to be more obvious in summer and autumn (Figure 4). Although few remotely sensed SIF studies have reported midday depression in SIF likely due to the lack of continuous, high temporal-resolution SIF measurements, the midday reduction in chlorophyll fluorescence emissions has been widely reported in many studies at leaf level (Martínez-Ferri et al., 2000; Raschke & Resemann, 1986; Špunda et al., 2005), which attributed this phenomenon to both stomatal and non-stomatal limitations from environmental stresses such as excess light and high VPD. Excess absorbed solar energy at midday increases energy allocation to non-radiative heat dissipation, which leads to reduced energy allocation to photochemistry and fluorescence, resulting in the midday depression in fluorescence (Demmig-Adams, 1990; Martínez-Ferri et al., 2000). The depression also occurs when the plant suffers from moisture stress with VPD exceeding the threshold (Raschke & Resemann, 1986). The midday depression in SIF from our measurements in mangroves corresponded to midday environmental stresses including excess light (Figure 2e) and high VPD (Figure 2g). Higher midday light/VPD/temperature around noon (Figures 2e–2g) might explain why midday depression in SIF was more obvious in summer and autumn.

In comparison, midday depression in GPP was not as obvious as that in SIF (Figure 4). Same with SIF, the extent of midday depression in GPP varied across seasons with relatively stronger suppression in summer and autumn (i.e., change from a humped phase to a stationary phase; Figures 4c and 4d). The reasons

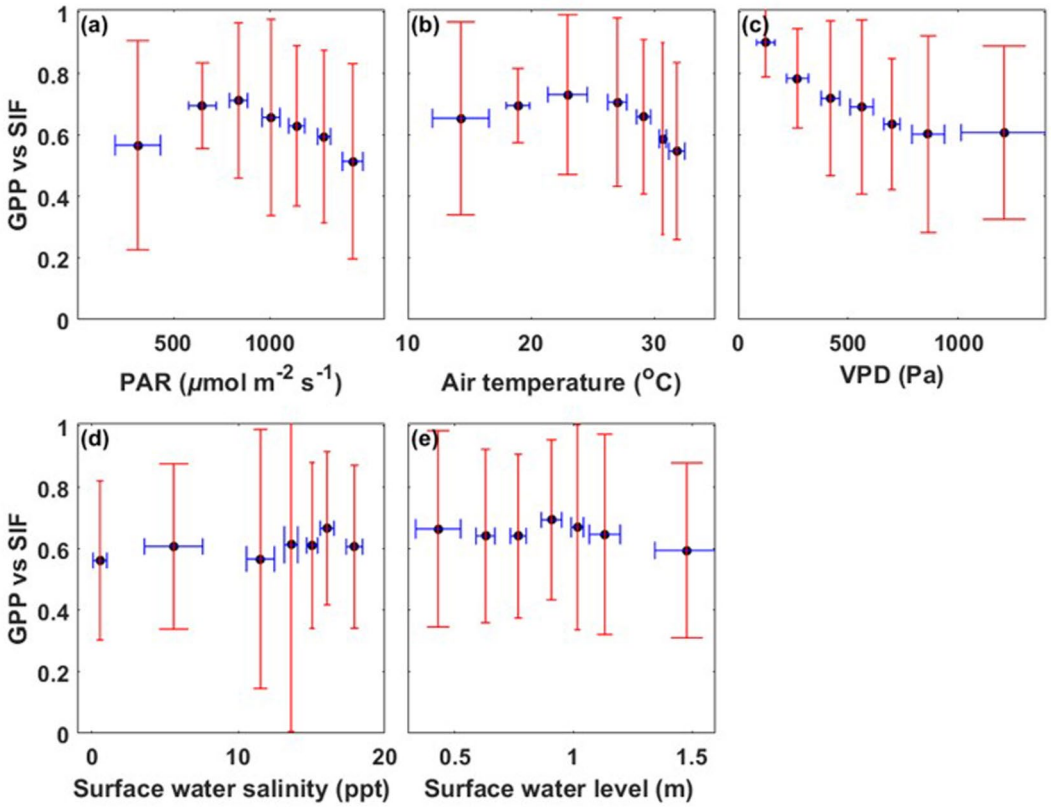

Figure 6. Influences of environmental factors on the correlation between 30-min GPP and SIF. Pearson's correlation coefficients were calculated for each single day and then grouped by daily values of environmental factors. The daily mean values were used for the environmental factors except surface water level (using daily maximum values). The vertical and horizontal error bars indicated standard deviations of SIF-GPP correlations and environmental factors, respectively. GPP, gross primary productivity; PAR, photosynthetically active radiation; SIF: sun-induced chlorophyll fluorescence; VPD, vapor pressure deficit.

why the extent of midday depression differed between GPP and SIF are manifold. First, the absorbed solar energy may also be consumed by non-radiative heat dissipation in addition to that used for SIF and photosynthetic activity, and thus there is no universal scaling relationship between SIF and GPP. Several studies have attributed the midday SIF depression to higher non-radiative heat dissipation (Li et al., 2000; Peguero-Pina et al., 2008; Paul-Limoges et al., 2018). Higher midday non-radiative heat dissipation was also supported by our previous study showing lower PRI at midday hours for the same mangrove forests (Zhu et al., 2019), since lower PRI corresponded to stronger non-radiative heat dissipation via xanthophyll cycle (Gamon et al., 1992). Second, although SIF is directly coupled to photosynthetic activity during light reactions, the whole physiological processes involved in SIF (light reactions only) and GPP (both light and carbon reactions) are not the same (Gu et al., 2019), and thus they are very likely subjected to different environmental controls (Porcar-Castell et al., 2014). Frequent cloud formation during the midday in subtropical coastal region leads to a decrease in PAR but an increase in LUE (due to higher fraction of diffuse radiation) (Barr et al., 2010; Gu et al., 2003). The combination of these two canceling effects might help to explain the relatively stationary GPP around noon especially in summer and autumn (Figures 4c and 4d). Third, it could also result from the difference in horizontal and vertical footprint sizes between SIF and EC systems. For horizontal footprint, SIF signal had a much smaller footprint (~3 m in diameter for tower-based SIF vs. ~100 m for tower-based GPP), and thus it is not a surprise that SIF was generally more sensitive to environmental stresses than GPP. For vertical footprint, tower-based SIF signals mainly represented the top-canopy leaves exposed to heavier environmental stresses around noon (e.g., high light, temperature, and VPD) than the leaves lower in the canopy, while tower-based GPP from EC measurements represented ecosystem carbon assimilation integrated over the whole canopy. Therefore, tower-based SIF was more likely affected by environmental stresses around noon than tower-based GPP, leading to their midday mismatch.

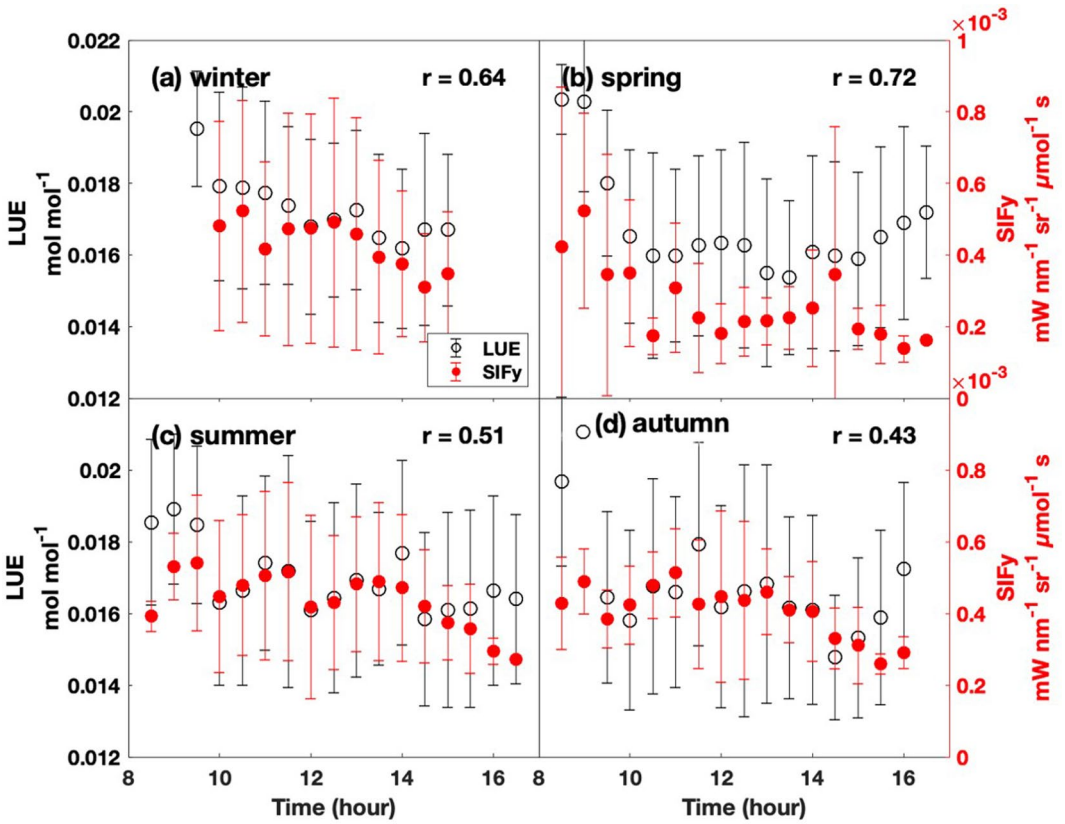

Figure 7. Diurnal variations in seasonally mean LUE and SIF_y across seasons: (a) winter, (b) spring, (c) summer, and (d) autumn. Markers and error bars represented mean values and standard deviations, respectively. Pearson's correlation coefficients (r) between diurnal mean LUE and SIF_y were calculated for each season (all coefficients were statistically significant at $p < 0.05$). Note the data with solar elevation angle <30° were excluded via quality control. LUE, light use efficiency; SIF_y, quantum yield of sun-induced chlorophyll fluorescence.

The analysis on the impact of the environmental factors on the SIF-GPP relationship revealed that the strengths of the SIF-GPP link varied across environmental gradients (Figure 6). Among these environmental factors, VPD was the only one exerting statistically significant ($p < 0.05$) negative effect on the SIF-GPP correlation, where lower VPD corresponded to stronger SIF-GPP correlation. The SIF-GPP correlation tended to be affected by PAR and air temperature, where the correlation peaked at medium PAR and air temperature. There was no indication that the SIF-GPP correlation was regulated by surface water salinity or surface water level. It is possible that tidal salinity at this field site (0–18 ppt for daily salinity) was not high enough to cause apparent salinity inhibition of mangrove photosynthesis, which usually occurs with daily salinity > 15 ppt (Barr et al., 2013; Cui et al., 2018). Although the environmental impacts on the SIF-GPP correlation differed in strength, as a whole the SIF-GPP correlations tended to be lower under atmospheric stresses (i.e., high PAR, air temperature and VPD), which was consistent with previous studies showing that the occurrence of environmental stresses decoupled the relationship between SIF and plant physiological dynamics (Atherton et al., 2016; Lu et al., 2018).

4.2. The SIF_y-LUE Link and Its Environmental Controls

In contrast with widely reported positive relationship between SIF and GPP across ecosystems and platforms, there is a lack of consensus regarding the functional relationship between SIF_y and LUE (Miao et al., 2018). Positive correlations (Verma et al., 2017; Yang et al., 2015), negative correlations (Damm et al., 2010), and even both of them (Miao et al., 2018; Zhang et al., 2016) have been found in previous studies on the SIF_y-LUE link across the time scales. It is not a surprise the SIF_y-LUE relationship is more variable than the SIF-GPP relationships, since the influence of APAR with much larger temporal variation has been

excluded in the former. From the physiological perspective, it can be possible to have both positive and negative SIF_y-LUE relationship since the proportion of absorbed energy flowing along each of the energy partitioning pathways can be dynamic and under various physiological controls. Porcar-Castell et al. (2014) discussed the physiological processes that control the energy partitioning in details at the photosystem level, and suggested a clear two-phased inverted "V" relationship between quantum yields of fluorescence and photochemistry over the course of a day based on leaf-level pulse amplitude-modulated (PAM) fluorescence measurements: (1) inversely proportional under low light phase; and (2) directly proportional under high light phase. Under low light, the change in photochemistry yield are dominated by photochemical quenching (PQ) with low and constant non-photochemical quenching (NPQ), while under high light the change in photochemistry yield are dominated by NPQ with constant PQ. Since decreasing PQ and increasing NPQ have opposite effects on fluorescence yield, it generates a two-phased "V" relationship between fluorescence yield and photochemistry yield (Porcar-Castell et al., 2014).

Although it may not be meaningful to directly compare canopy-level SIF measurements (non-steady SIF) with leaf-level PAM fluorescence measurement (steady SIF), we did observe a similar two-phased diurnal relationship between SIF_y and LUE (Figure 7). The difference in diurnal variations between SIF_y and LUE supports the notion that the functional relationship between SIF_y and LUE depends on light conditions (Miao et al., 2018; Zhang et al., 2016). Another possible reason explaining the divergence between SIF_y and LUE at early morning/late afternoon is that, at lower solar elevations, larger proportion of light is absorbed by within-canopy leaves rather than by top-canopy leaves, resulting in less detected SIF emissions due to the within-canopy re-absorption effect (Du et al., 2017; Porcar-Castell et al., 2014). The escape probability of emitted fluorescence was not considered here, and thus it was possible that the observed diverge between SIF_y and LUE at early morning/late afternoon might have been magnified by ignoring the escape probability that can vary substantially over the day (Yang & van der Tol, 2018; Zeng et al., 2019).

4.3. Implications and Uncertainties

The asymptotic behavior of the SIF-GPP relationship at diurnal scale (increasing SIF vs. saturating GPP) indicates that the increase in SIF is faster than the increase in GPP under light-saturating conditions. For this reason, we expect that the estimation of GPP from sporadic spaceborne and airborne SIF measurements (usually under light-saturating conditions) would be higher than the actual values if a linear SIF-GPP empirical relationship was assumed. It should be cautious to establish functional relationship between SIF and GPP since it could be time scale-dependent. The mismatch of midday depression between SIF and GPP under high light observed from our results also suggests that the retrieval of SIF-GPP relationship from those sporadic SIF measurements could contain biases.

Although the SIF-GPP correlations are not as strong as those reported by previous ground-based SIF studies, our results demonstrate the potential of SIF in indicating mangrove canopy GPP with comparable performance of PRI. This confirms that SIF can serve an important complement to reflectance-based VIs in indicating mangrove carbon fluxes. It should be noted that previous ground-based SIF mainly focused on vegetation experiencing either seasonally distinct canopy structure or temperature variation over the course of the year, while evergreen mangroves in this study are experiencing indistinct canopy structure and small temperature variation. This can partially explain why the SIF-GPP correlation in mangrove forests is relatively weaker. Both of the midday depression in SIF and the variation in SIF_y at the diurnal scale suggest that SIF might be highly sensitive to various environmental stresses, which reveals the potential of applying SIF to examine the influences of various types of stresses on mangrove carbon fluxes.

Although tower-based continuous measurements of both SIF and EC systems enabled us to examine the SIF-GPP and SIF_y-LUE relationships and to disentangle the confounding effects of various environmental factors, several uncertainties are involved in field experiment setups and data processing/analyses. First, the direct comparison between tower-based SIF and GPP suffers from the difference in footprint sizes (both in horizontal and vertical dimensions) between SIF and EC instrumentations. The impacts of the difference in horizontal footprint sizes were not considered in data analyses of this study, but future studies should examine how this "horizontal mismatch" affects the SIF-GPP correlations. Tower-based SIF signals predominately come from top-canopy leaves because of the re-absorption of emitted SIF within the canopy (Du et al., 2017; Porcar-Castell et al., 2014), while GPP represents carbon assimilations integrated over the

whole canopy. This "vertical mismatch" may affect the empirical relationships and their sensitivities to environmental stresses. Second, tower-based SIF measurements are affected by changing fractions of sunlit and shaded leaves over the course of a day (He et al., 2017; Tol et al., 2009; Zhang et al., 2020), and this sun-viewing-geometry issue requires further investigations (Liu et al., 2016; Pinto et al., 2017). Third, there is a growing recognition of the importance of escape probability of emitted fluorescence, which is highly dependent on canopy structure and affects the amount and temporal variation of fluorescence "seen" by the spectrometer (Yang & van der Tol, 2018; Zeng et al., 2019). The retrieved SIF could be smaller than actual fluorescence emissions by ignoring the escape probability, which propagates uncertainty to the analyses of temporal variation of SIF and the SIF-GPP correlations. This limitation needs further investigation in future studies. Fourth, the choice of various SIF retrieval algorithms could affect our data analyses. To examine the impact of algorithms on the retrieved SIF, we tried another commonly used algorithm, 3FLD (Meroni et al., 2009), and the comparison showed little difference between 3FLD-based and SFM-based SIF (Figure S2), which supported the reliability of retrieved SIF. Fifth, the dismissal of atmospheric absorption (a 7-m distance between fiber optics and mangrove canopy as in this study) of reflected canopy radiance could bias the retrieved SIF (Liu et al., 2017). A rough analysis of the influence of atmospheric absorption on SFM-based SIF retrieval (assuming 1% decrease in upwelling atmospheric transmittance for a 7-m distance according to Liu et al. [2017]) indicated that the difference was negligible (<2%) between retrieved SIF with and without considering atmospheric absorption. Sixth, further attentions should be paid to the uncertainties associated with the partitioning approaches for EC-derived GPP (Reichstein et al., 2005) and the applicability of the approaches in tide-affected mangrove wetlands (Barr et al., 2013). See Wohlfahrt and Gu (2015) for a comprehensive discussion on the potential difference between EC-derived and "true" photosynthesis as well as the issues associated with the partitioning approaches. Last but not least, our data analyses suffered from the sparseness of the data and resultant sampling biases over the day and the season due to instrument failure and quality control (e.g., low data availability in winter, and under-sampling in early mornings and late afternoons), and thus improvements of instrumentations and maintenance for more data availability are highly need to further confirm these findings.

5. Conclusions

Qualitative and quantitative analyses have been conducted here to explore the temporal dynamics of SIF and GPP as well as their link under various environmental conditions at a subtropical mangrove forest of southeastern China, based on 1-year continuous and concurrent time-series measurements from tower-based hyperspectral and EC systems. Both of the SIF-GPP and the SIF_y-LUE relationships were examined to assess the capability of SIF for tracking mangrove photosynthesis at diurnal and seasonal time scales. The main findings are summarized as follows. (1) The temporal variations of SIF and GPP shared overall similar changing patterns at diurnal and seasonal time scales. (2) The SIF-GPP correlations was comparable with the PRI-GPP correlations and thus SIF can serve a potential remotely sensed indicator of mangrove canopy GPP. (3) The functional relationship between SIF and GPP in mangroves might be time scale-dependent with more nonlinear and linear at diurnal and seasonal time scales, respectively. (4) Midday depression in SIF was observed in mangroves when environmental stresses occurred around noon (including excess light and high VPD), and the strength of the SIF-GPP relationship was affected by changing environmental conditions. (5) The SIF_y-LUE relationship was temporally more dynamic than the SIF-GPP relationship, and SIF and LUE tended to match during midday hours but diverge from each other during morning and afternoon hours. This study provides the first, high temporal-resolution, continuous SIF measurements in mangroves and highlights the importance of characterizing the impacts of environmental conditions on the SIF-GPP relationship. Future studies should take into account these issues in order to reduce the uncertainty in estimating GPP from remotely sensed SIF measurements.

Conflict of Interest

The authors declare no conflicts of interest relevant to this study.

Data Availability Statement

The data necessary to reproduce key findings in this study can be accessed at http://doi.org/10.5281/zenodo.4543631.

Acknowledgments
The authors thank Yaqing Lu, Kangming Chen, Chenyang Sun, Chengjuan Zheng, and Guanmin Huang for their help in the fieldwork and data quality control. The authors thank the Zhangjiang Estuary Mangrove National Nature Reserve for its long-term support to our ecological research program. The authors also thank ChinaFLUX and the U.S.-China Carbon Consortium (USCCC) for helpful discussions and exchange of ideas. This study was supported by the National Natural Science Foundation of China (31600368), the National Key Research and Development Program of China (2017YFC0506102), the Natural Science Foundation of Fujian Province, China (2017J01069, 2020J01112079), the Youth Innovation Foundation of Xiamen, China (3502Z20206038), the Fundamental Research Funds for the Central Universities of China (20720180118, 20720190104), the Key Laboratory of the Coastal and Wetland Ecosystems (WELRI201601), and the State Key Laboratory of Marine Environmental Science (MELRI1603).

References

Ač, A., Malenovský, Z., Olejníčková, J., Gallé, A., Rascher, U., & Mohammed, G. (2015). Meta-analysis assessing potential of steady-state chlorophyll fluorescence for remote sensing detection of plant water, temperature and nitrogen stress. *Remote Sensing of Environment*, *168*, 420–436.

Alongi, D. M. (2009). *The energetics of mangrove forests*. Netherlands: Springer.

Alongi, D. M. (2012). Carbon sequestration in mangrove forests. *Carbon Management*, *3*(3), 313–322. https://doi.org/10.4155/cmt.12.20

Alongi, D. M. (2014). Carbon cycling and storage in mangrove forests. *The Annual Review of Marine Science*, *6*, 195–219. https://doi.org/10.1146/annurev-marine-010213-135020

Atherton, J., Nichol, C. J., & Porcar-Castell, A. (2016). Using spectral chlorophyll fluorescence and the photochemical reflectance index to predict physiological dynamics. *Remote Sensing of Environment*, *176*, 17–30. https://doi.org/10.1016/j.rse.2015.12.036

Atwood, T. B., Connolly, R. M., Almahasheer, H., Carnell, P. E., Duarte, C. M., Ewers Lewis, C. J., et al. (2017). Global patterns in mangrove soil carbon stocks and losses. *Nature Climate Change*, *7*(7), 523. https://doi.org/10.1038/nclimate3326

Baldocchi, D., Falge, E., Gu, L., Olson, R., Hollinger, D., Running, S., et al. (2001). FLUXNET: A new tool to study the temporal and spatial variability of ecosystem-scale carbon dioxide, water vapor, and energy flux densities. *The Bulletin of the American Meteorological Society*, *82*(11), 2415–2434. https://doi.org/10.1175/1520-0477(2001)082<2415:fantts>2.3.co;2

Ball, M. C. (1996). Comparative ecophysiology of mangrove forest and tropical lowland moist rainforest, In S. S. Mulkey, R. L. Chazdon, & A. P. Smith (Eds.), *Tropical forest plant ecophysiology* (pp. 461–496). Boston, MA: Springer.

Barr, J. G., Engel, V., Fuentes, J. D., Fuller, D. O., & Kwon, H. (2013). Modeling light use efficiency in a subtropical mangrove forest equipped with CO_2 eddy covariance. *Biogeosciences*, *10*(3), 2145–2158. https://doi.org/10.5194/bg-10-2145-2013

Barr, J. G., Engel, V., Fuentes, J. D., Zieman, J. C., O'Halloran, T. L., Smith, T. J., & Anderson, G. H. (2010). Controls on mangrove forest-atmosphere carbon dioxide exchanges in western Everglades National Park. *Journal of Geophysical Research*, *115*(G2). https://doi.org/10.1029/2009jg001186

Cogliati, S., Rossini, M., Julitta, T., Meroni, M., Schickling, A., Burkart, A., et al. (2015). Continuous and long-term measurements of reflectance and sun-induced chlorophyll fluorescence by using novel automated field spectroscopy systems. *Remote Sensing of Environment*, *164*, 270–281. https://doi.org/10.1016/j.rse.2015.03.027

Crase, B., Vesk, P. A., Liedloff, A., & Wintle, B. A. (2015). Modeling both dominance and species distribution provides a more complete picture of changes to mangrove ecosystems under climate change. *Global Change Biology*, *21*(8), 3005–3020. https://doi.org/10.1111/gcb.12930

Cui, X., Liang, J., Lu, W., Chen, H., Liu, F., Lin, G., et al. (2018). Stronger ecosystem carbon sequestration potential of mangrove wetlands with respect to terrestrial forests in subtropical China. *Agricultural and Forest Meteorology*, *249*, 71–80. https://doi.org/10.1016/j.agrformet.2017.11.019

Damm, A., Elbers, J., Erler, A., Gioli, B., Hamdi, K., Hutjes, R., et al. (2010). Remote sensing of sun-induced fluorescence to improve modeling of diurnal courses of gross primary production (GPP). *Global Change Biology*, *16*(1), 171–186. https://doi.org/10.1111/j.1365-2486.2009.01908.x

Damm, A., Guanter, L., Laurent, V. C. E., Schaepman, M. E., Schickling, A., & Rascher, U. (2014). FLD-based retrieval of sun-induced chlorophyll fluorescence from medium spectral resolution airborne spectroscopy data. *Remote Sensing of Environment*, *147*, 256–266. https://doi.org/10.1016/j.rse.2014.03.009

Damm, A., Guanter, L., Paul-Limoges, E., van der Tol, C., Hueni, A., Buchmann, N., et al. (2015). Far-red sun-induced chlorophyll fluorescence shows ecosystem-specific relationships to gross primary production: An assessment based on observational and modeling approaches. *Remote Sensing of Environment*, *166*, 91–105. https://doi.org/10.1016/j.rse.2015.06.004

Demmig-Adams, B. (1990). Carotenoids and photoprotection in plants: A role for the xanthophyll zeaxanthin. *Biochimica et Biophysica Acta (BBA) – Bioenergetics*, *1020*(1), 1–24. https://doi.org/10.1016/0005-2728(90)90088-l

Du, S., Liu, L., Liu, X., & Hu, J. (2017). Response of canopy solar-induced chlorophyll fluorescence to the absorbed photosynthetically active radiation absorbed by chlorophyll. *Remote Sensing*, *9*(9), 911. https://doi.org/10.3390/rs9090911

Frankenberg, C., Fisher, J. B., Worden, J., Badgley, G., Saatchi, S. S., Lee, J.-E., et al. (2011). New global observations of the terrestrial carbon cycle from GOSAT: Patterns of plant fluorescence with gross primary productivity. *Geophysical Research Letters*, *38*(17). https://doi.org/10.1029/2011gl048738

Gamon, J. A. (2015). Reviews and syntheses: Optical sampling of the flux tower footprint. *Biogeosciences*, *12*(14), 4509–4523. https://doi.org/10.5194/bg-12-4509-2015

Gamon, J. A., Peñuelas, J., & Field, C. B. (1992). A narrow-waveband spectral index that tracks diurnal changes in photosynthetic efficiency. *Remote Sensing of Environment*, *41*(1), 35–44. https://doi.org/10.1016/0034-4257(92)90059-s

Garbulsky, M. F., Peñuelas, J., Gamon, J., Inoue, Y., & Filella, I. (2011). The photochemical reflectance index (PRI) and the remote sensing of leaf, canopy and ecosystem radiation use efficiencies: A review and meta-analysis. *Remote Sensing of Environment*, *115*(2), 281–297. https://doi.org/10.1016/j.rse.2010.08.023

Gitelson, A. A., & Gamon, J. A. (2015). The need for a common basis for defining light-use efficiency: Implications for productivity estimation. *Remote Sensing of Environment*, *156*, 196–201. https://doi.org/10.1016/j.rse.2014.09.017

Goulas, Y., Fournier, A., Daumard, F., Champagne, S., Ounis, A., Marloie, O., & Moya, I. (2017). Gross primary production of a wheat canopy relates stronger to far red than to red solar-induced chlorophyll fluorescence. *Remote Sensing*, *9*(1). https://doi.org/10.3390/rs9010097

Guanter, L., Zhang, Y., Jung, M., Joiner, J., Voigt, M., Berry, J. A., et al. (2014). Global and time-resolved monitoring of crop photosynthesis with chlorophyll fluorescence. *Proceedings of the National Academy of Sciences of the United States of America*, *111*(14), E1327–E1333.

Gu, L., Baldocchi, D. D., Wofsy, S. C., William Munger, J., Michalsky, J. J., Urbanski, S. P., & Boden, T. A. (2003). Response of a deciduous forest to the Mount Pinatubo eruption: Enhanced photosynthesis. *Science*, *299*(5615), 2035–2038. https://doi.org/10.1126/science.1078366

Gu, L., Han, J., Wood, J. D., Chang, C. Y. Y., & Sun, Y. (2019). Sun-induced Chl fluorescence and its importance for biophysical modeling of photosynthesis based on light reactions. *New Phytologist*, *223*(3), 1179–1191. https://doi.org/10.1111/nph.15796

He, L., Chen, J. M., Liu, J., Mo, G., & Joiner, J. (2017). Angular normalization of GOME-2 Sun-induced chlorophyll fluorescence observation as a better proxy of vegetation productivity. *Geophysical Research Letters*, *44*, 5691–5699. https://doi.org/10.1002/2017GL073708

Howard, J., Sutton-Grier, A., Herr, D., Kleypas, J., Landis, E., Mcleod, E. (2017). Clarifying the role of coastal and marine systems in climate mitigation. *Frontiers in Ecology and the Environment*, *15*(1), 42–50.

Huete, A., Didan, K., Miura, T., Rodriguez, E. P., Gao, X., & Ferreira, L. G. (2002). Overview of the radiometric and biophysical performance of the MODIS vegetation indices. *Remote Sensing of Environment*, *83*(1–2), 195–213.

Jiang, S., Lu, H., Liu, J., Lin, Y., Dai, M., & Yan, C. (2018). Influence of seasonal variation and anthropogenic activity on phosphorus cycling and retention in mangrove sediments: A case study in China. *Estuarine Coastal and Shelf Science*, *202*, 134–144.

Lee, J.-E., Berry, J. A., van der Tol, C., Yang, X., Guanter, L., Damm, A., et al. (2015). Simulations of chlorophyll fluorescence incorporated into the Community Land Model version 4. *Global Change Biology*, *21*(9), 3469–3477.

Lin, P. (2001). *The comprehensive report of science investigation on the natural reserve of mangrove wetland of Zhangjiang Estuary in Fujian*. Xiamen University Press.

Liu, J., Chen, J. M., Cihlar, J., & Park, W. M. (1997). A process-based boreal ecosystem productivity simulator using remote sensing inputs. *Remote Sensing of Environment*, *62*, 158–175.

Liu, J., & Lai, D. Y. (2019). Subtropical mangrove wetland is a stronger carbon dioxide sink in the dry than wet seasons. *Agricultural and Forest Meteorology*, *278*, 107644.

Liu, L., Guan, L., & Liu, X. (2017). Directly estimating diurnal changes in GPP for C3 and C4 crops using far-red sun-induced chlorophyll fluorescence. *Agricultural and Forest Meteorology*, *232*, 1–9.

Liu, L., Liu, X., Wang, Z., & Zhang, B. (2016). Measurement and analysis of bidirectional SIF emissions in wheat canopies. *IEEE Transactions on Geoscience and Remote Sensing*, *54*(5), 2640–2651.

Liu, X., Liu, L., Hu, J., & Du, S. (2017). Modeling the footprint and equivalent radiance transfer path length for tower-based hemispherical observations of chlorophyll fluorescence. *Sensors*, *17*(5).

Li, X.-P., Björkman, O., Shih, C., Grossman, A. R., Rosenquist, M., Jansson, S., & Niyogi, K. K. (2000). A pigment-binding protein essential for regulation of photosynthetic light harvesting. *Nature*, *403*(6768), 391.

Li, X., Xiao, J., & He, B. (2018). Chlorophyll fluorescence observed by OCO-2 is strongly related to gross primary productivity estimated from flux towers in temperate forests. *Remote Sensing of Environment*, *204*, 659–671.

Lu, X., Liu, Z., An, S., Miralles, D. G., Maes, W., Liu, Y., Tang, J. (2018). Potential of solar-induced chlorophyll fluorescence to estimate transpiration in a temperate forest. *Agricultural and Forest Meteorology*, *252*, 75–87.

Magney, T. S., Bowling, D. R., Logan, B. A., Grossmann, K., Stutz, J., Blanken, P. D., et al. (2019). Mechanistic evidence for tracking the seasonality of photosynthesis with solar-induced fluorescence. *Proceedings of the National Academy of Sciences of the United States of America*. *116*(24), 11640–11645.

Martínez-Ferri, E., Balaguer, L., Valladares, F., Chico, J., & Manrique, E. (2000). Energy dissipation in drought-avoiding and drought-tolerant tree species at midday during the Mediterranean summer. *Tree Physiology*, *20*(2), 131–138.

Maxwell, K., & Johnson, G. N. (2000). Chlorophyll fluorescence – A practical guide. *Journal of Experimental Botany*, *51*(345), 659–668.

Mercado, L. M., Bellouin, N., Sitch, S., Boucher, O., Huntingford, C., Wild, M., & Cox, P. M. (2009). Impact of changes in diffuse radiation on the global land carbon sink. *Nature*, *458*, 1014.

Meroni, M., Rossini, M., Guanter, L., Alonso, L., Rascher, U., Colombo, R., & Moreno, J. (2009). Remote sensing of solar-induced chlorophyll fluorescence: Review of methods and applications. *Remote Sensing of Environment*, *113*(10), 2037–2051.

Miao, G., Guan, K., Yang, X., Bernacchi, C. J., Berry, J. A., DeLucia, E. H., et al. (2018). Sun-induced chlorophyll fluorescence, photosynthesis, and light use efficiency of a soybean field from seasonally continuous measurements. *Journal of Geophysical Research: Biogeosciences*, *123*(2), 610–623. https://doi.org/10.1002/2017JG004180

Murray, F. W. (1966). *On the computation of saturation vapor pressure*. Santa Monica, CA: RAND Corp.

Myneni, R. B., & Williams, D. L. (1994). On the relationship between FAPAR and NDVI. *Remote Sensing of Environment*, *49*(3), 200–211.

Nellemann, C., & Corcoran, E. (2009). *Blue carbon: The role of healthy oceans in binding carbon: A rapid response assessment*. UNEP/Earthprint.

Nichol, C. J., Drolet, G., Porcar-Castell, A., Wade, T., Sabater, N., Middleton, E. M., et al. (2019). Diurnal and seasonal solar induced chlorophyll fluorescence and photosynthesis in a boreal scots pine canopy. *Remote Sensing*, *11*(3), 273.

Paul-Limoges, E., Damm, A., Hueni, A., Liebisch, F., Eugster, W., Schaepman, M. E., & Buchmann, N. (2018). Effect of environmental conditions on sun-induced fluorescence in a mixed forest and a cropland. *Remote Sensing of Environment*, *219*, 310–323.

Peguero-Pina, J. J., Morales, F., Flexas, J., Gil-Pelegrín, E., & Moya, I. (2008). Photochemistry, remotely sensed physiological reflectance index and de-epoxidation state of the xanthophyll cycle in Quercus coccifera under intense drought. *Oecologia*, *156*(1), 1.

Perez-Priego, O., Zarco-Tejada, P. J., Miller, J. R., Sepulcre-Canto, G., & Fereres, E. (2005). Detection of water stress in orchard trees with a high-resolution spectrometer through chlorophyll fluorescence in-filling of the O_2-A band. *IEEE Transactions on Geoscience and Remote Sensing*, *43*(12), 2860–2869.

Pinto, F., Müller-Linow, M., Schickling, A., Cendrero-Mateo, M. P., Ballvora, A., & Rascher, U. (2017). Multiangular observation of canopy Sun-induced chlorophyll fluorescence by combining imaging spectroscopy and stereoscopy. *Remote Sensing*, *9*(5).

Porcar-Castell, A., Tyystjärvi, E., Atherton, J., van der Tol, C., Flexas, J., Pfündel, E. E., Moreno, J., et al. (2014). Linking chlorophyll a fluorescence to photosynthesis for remote sensing applications: mechanisms and challenges. *Journal of Experimental Botany*, *65*(15), 4065–4095.

Raschke, K., & Resemann, A. (1986) The midday depression of CO_2 assimilation in leaves of Arbutus unedo L. Diurnal changes in photosynthetic capacity related to changes in temperature and humidity. *Planta*, *168*(4), 546–558.

Reichstein, M., Falge, E., Baldocchi, D., Papale, D., Aubinet, M., Berbigier, P., et al. (2005). On the separation of net ecosystem exchange into assimilation and ecosystem respiration: Review and improved algorithm. *Global Change Biology*, *11*(9), 1424–1439.

Song, C., White, B. L., & Heumann, B. W. (2011). Hyperspectral remote sensing of salinity stress on red (*Rhizophora mangle*) and white (*Laguncularia racemosa*) mangroves on Galapagos Islands. *Remote Sensing Letters*, *2*(3), 221–230.

Špunda, V., Kalina, J., Urban, O., Luis, V. C., Sibisse, I., Puértolas, J., et al. (2005). Diurnal dynamics of photosynthetic parameters of Norway spruce trees cultivated under ambient and elevated CO_2: The reasons of midday depression in CO_2 assimilation. *Plant Science*, *168*(5), 1371–1381.

Sun, Y., Frankenberg, C., Jung, M., Joiner, J., Guanter, L., Köhler, P., & Magney, T. (2018). Overview of solar-induced chlorophyll fluorescence (SIF) from the orbiting carbon observatory-2: Retrieval, cross-mission comparison, and global monitoring for GPP. *Remote sensing of Environment*. *209*: 808–823.

Sun, Y., Frankenberg, C., Wood, J. D., Schimel, D. S., Jung, M., Guanter, L., et al. (2017). OCO-2 advances photosynthesis observation from space via solar-induced chlorophyll fluorescence. *Science*, *358*(6360). eaam5747.

Tol, C., Verhoef, W., Timmermans, J., Verhoef, A., & Su, Z. (2009). An integrated model of soil-canopy spectral radiances, photosynthesis, fluorescence, temperature and energy balance. *Biogeosciences*, *6*(12), 3109–3129.

Turner, D. P., Urbanski, S., Bremer, D., Wofsy, S. C., Meyers, T., Gower, S. T., & Gregory, M. (2003). A cross-biome comparison of daily light use efficiency for gross primary production. *Global Change Biology*, *9*(3), 383–395.

Verma, M., Schimel, D., Evans, E., Frankenberg, C., Beringer, J., Drewry, D. T., et al. (2017). Effect of environmental conditions on the relationship between solar-induced fluorescence and gross primary productivity at an OzFlux grassland site. *Journal of Geophysical Research: Biogeosciences*, *122*(3), 716–733. https://doi.org/10.1002/2016JG003580

Wohlfahrt, G., & Gu, L. (2015). The many meanings of gross photosynthesis and their implication for photosynthesis research from leaf to globe. *Plant, Cell and Environment*, *38*(12), 2500–2507.

Yang, H., Yang, X., Zhang, Y., Heskel, M. A., Lu, X., Munger, J. W., et al. (2017). Chlorophyll fluorescence tracks seasonal variations of photosynthesis from leaf to canopy in a temperate forest. *Global Change Biology*, *23*(7), 2874–2886.

Yang, P., & van der Tol, C. (2018). Linking canopy scattering of far-red sun-induced chlorophyll fluorescence with reflectance. *Remote Sensing of Environment*, *209*, 456–467.

Yang, X., Tang, J., Mustard, J. F., Lee, J-E, Rossini, M., Joiner, J., et al. (2015). Solar-induced chlorophyll fluorescence that correlates with canopy photosynthesis on diurnal and seasonal scales in a temperate deciduous forest. *Geophysical Research Letters*, *42*(8), 2977–2987. https://doi.org/10.1002/2015GL063201

Zarco-Tejada, P. J., Catalina, A., González, M. R., & Martín, P. (2013). Relationships between net photosynthesis and steady-state chlorophyll fluorescence retrieved from airborne hyperspectral imagery. *Remote Sensing of Environment*, *136*, 247–258.

Zeng, Y., Badgley, G., Dechant, B., Ryu, Y., Chen, M., & Berry, J. A. (2019). A practical approach for estimating the escape ratio of near-infrared solar-induced chlorophyll fluorescence. *Remote Sensing of Environment*, *232*, 111209.

Zhang, M., Yu, G.-R., Zhuang, J., Gentry, R., Fu, Y.-L., Sun, X.-M., et al. (2011). Effects of cloudiness change on net ecosystem exchange, light use efficiency, and water use efficiency in typical ecosystems of China. *Agricultural and Forest Meteorology*, *151*(7), 803–816.

Zhang, Y., Guanter, L., Berry, J. A., van der Tol, C., Yang, X., Tang, J., & Zhang, F. (2016). Model-based analysis of the relationship between sun-induced chlorophyll fluorescence and gross primary production for remote sensing applications. *Remote Sensing of Environment*, *187*, 145–155.

Zhang, Z., Chen, J. M., Guanter, L., He, L., & Zhang, Y. (2019). From canopy-leaving to total canopy far-red fluorescence emission for remote sensing of photosynthesis: First results from TROPOMI. *Geophysical Research Letters*, *46*, 12030–12040. https://doi.org/10.1029/2019GL084832

Zhang, Z., Zhang, Y., Zhang, Q., Chen, J. M., Porcar-Castell, A., Guanter, L., et al. (2020). Assessing bi-directional effects on the diurnal cycle of measured solar-induced chlorophyll fluorescence in crop canopies. *Agricultural and Forest Meteorology*, *295*, 108147.

Zhu, X., Hou, Y., Weng, Q., & Chen, L. (2019). Integrating UAV optical imagery and LiDAR data for assessing the spatial relationship between mangrove and inundation across a subtropical estuarine wetland. *ISPRS Journal of Photogrammetry and Remote Sensing*, *149*, 146–156.

Zhu, X., Song, L., Weng, Q., & Huang, G. (2019). Linking in situ photochemical reflectance index measurements with mangrove carbon dynamics in a subtropical coastal wetland. *Journal of Geophysical Research: Biogeosciences*, *124*(6), 1714–1730. https://doi.org/10.1029/2019JG005022